



Serhii BURLAKA¹, Ihor KUPCHUK², Tetiana BORETSKA³, Yaroslav GONTARUK⁴,
Maryna MELNYK⁵

Optimizing the process of mixing diesel fuel and biofuel in a blade mixer to improve mixture quality

ABSTRACT: This research examines an important aspect of technological processes – the process of mixing diesel fuel and biofuel in a specially designed paddle mixer. The main goal is to optimize and improve the quality of the resulting mixture. The use of the FlowVision CFD (Computational Fluid Dynamics) program in this study is of great importance and helps to achieve significant results in the study and optimization of the diesel-biofuel mixing process. In the context of many industrial and technological processes, where efficient mixing of liquids plays an important role, turbulent mixing is of great importance. Optimal mixing not only improves the quality of products, but also ensures the unity of complex reactions and also helps to reduce the time of completion of the process. It is important to emphasize that the research focuses not only on the quantitative aspects of mixing but

✉ Corresponding Author: Ihor Kupchuk; e-mail: kupchuk.igor@i.ua

¹ Engineering and Technology Faculty, Vinnytsia National Agrarian University, Ukraine; ORCID iD: 0000-0002-4079-4867; e-mail: ipserhiy@gmail.com

² Engineering and Technology Faculty, Vinnytsia National Agrarian University, Ukraine; ORCID iD: 0000-0002-2973-6914; e-mail: kupchuk.igor@i.ua

³ Engineering and Technology Faculty, Vinnytsia National Agrarian University, Ukraine; ORCID iD: 0000-0002-7966-228X; e-mail: boreckatetana@gmail.com

⁴ Faculty of Management and Law, Vinnytsia National Agrarian University, Ukraine; ORCID iD: 0000-0002-7616-9422; e-mail: e050122015@gmail.com

⁵ Engineering and Technology Faculty, Vinnytsia National Agrarian University, Ukraine; ORCID iD: 0000-0001-8517-1690; e-mail: Marynab1611@gmail.com



© 2024. The Author(s). This is an open-access article distributed under the terms of the Creative Commons Attribution-ShareAlike International License (CC BY-SA 4.0, <http://creativecommons.org/licenses/by-sa/4.0/>), which permits use, distribution, and reproduction in any medium, provided that the Article is properly cited.

also on the study of the influence of the geometry of the mixer on the turbulent characteristics of the flow. This can lead to the development of new mixer designs aimed at maximizing the efficiency of the fuel mixing process, which, in turn, will help save resources and reduce emissions of harmful substances into the atmosphere. This research opens up prospects for further developments in the field of fuel blending technologies, which can lead to real improvements in production and sustainability. The discovery of new methods of optimal mixing of liquids in specially designed mixers can determine the future of energy efficiency and reduce the negative impact on the environment.

KEYWORDS: mixer geometry, numerical solution, turbulence, pressure gradient, turbulent flows

Introduction

Currently, technological processes in various branches of industry are being intensified. Modern automated systems, including various technical facilities, are used to ensure quality control and manage these processes. Field-level technical equipment, including automatic capillary viscometers, occupy the largest share of measurement error in these systems. It is still not possible to completely exclude the error of technical equipment of the first automation level, though it can be reduced (Galushchak 2015; Costa and Piazzullo 2018; Burlaka et al. 2021). Increasing the accuracy of measurements is an urgent task. For this purpose, it is necessary to study the hydrodynamic processes inside the space of capillary viscometers more deeply. Modern computational fluid dynamics (CFD) methods make it possible to solve this problem with fairly high accuracy (Aliiev et al. 2021).

Modeling is the basis of human cognition of the surrounding world. When conducting experiments, theoretical research, and even discussing our own actions, intentions, and conclusions, we actually perform modeling (Costa and Piazzullo 2018; Burlaka et al. 2021). The goals, tasks, tools, and modeling methods in these cases differ significantly from each other. Nevertheless, the general focus remains the same, i.e., obtaining new knowledge by testing (researching) some substitute for the real research object, namely, the model. In general, in a simplified way, modeling can be considered a certain experiment (Bandura et al. 2023). In the first case, its object is a material analog of the object under study. In the second case, the object of testing is a symbolic (mathematical) model. In the third case, it is the attitude of the community to the model under consideration (Galushchak O.O. and Galushchak D.O. 2014; Galushchak 2015; Gunko et al. 2021).

In particular, blade mixers are used in various industrial sectors, such as chemical, petrochemical, pharmaceutical, food, etc. However, despite a large amount of research on turbulent fluid mixing, some aspects of the relationship between the blade mixer geometry and turbulent characteristics have not been sufficiently elucidated and systematically investigated.

1. Materials and methods

Mixing diesel fuel and biofuel is an important step in biofuel production and the reduction of emissions of harmful substances into the atmosphere. Optimization of this process can significantly improve the quality of the final mixture and, therefore, increase the efficiency of fuel consumption. A detailed analysis of the mixing process using the FlowVision CFD program is expected to be carried out in our research.

One of the key elements of the mixer, which affects the characteristics of the turbulent flow and the intensity of liquid mixing, is its geometry. Geometric parameters of the blade mixer, e.g., the shape of blades, their length, the angle of inclination, as well as the configuration of the mixer as a whole, can significantly affect the processes of turbulent mixing of the liquid (Kaletnik and Yaropud 2023).

Despite numerous studies in the field of turbulent mixing, the issue of the influence of the geometry of the blade mixer on the characteristics of the turbulent flow and the intensity of liquid mixing remains insufficiently studied. It is known that various geometric parameters can change the structure of the turbulent flow. However, their exact relationships and regularities and turbulent characteristics remain incompletely clarified (Kaletnik and Yaropud 2021).

Thus, the main problem to be solved is a system analysis of the influence of the blade mixer geometry on the turbulence and the intensity of liquid mixing. Modeling is performed in the following sequence.

The development of a mathematical model of the mixing process involves defining the equations and parameters that describe the process of mixing diesel fuel and biofuel in the mixer (Kupchuk et al. 2022).

The equation of inseparability:

$$\frac{\partial \rho_g}{\partial t} + \vec{\nabla} \cdot (\rho_g V_g) = Q_{mass}^p \quad (1)$$

The equation of mass conservation for substance 1:

$$\frac{\partial (\rho_g Y_1)}{\partial t} + \vec{\nabla} \cdot (\rho_g V_g Y_1) = \vec{\nabla} \cdot \left(\left(\rho_g D_1 + \frac{\mu_t}{Sc_t} \right) \vec{\nabla} Y_1 \right) + Q_{mass}^p \quad (2)$$

The turbulent Schmidt number is equal to one:

$$Sc_t = \frac{\mu_t}{\rho_g D_t} = 1 \quad (3)$$

The mass concentration of Substance 0 is revealed from the condition:

$$Y_0 + Y_1 = 1 \quad (4)$$

The momentum conservation equation is as follows:

$$\frac{\partial(\rho_g V_g)}{\partial t} + \vec{\nabla} \cdot (\rho_g V_g \otimes V_g) = -\vec{\nabla} P + \vec{\nabla} \cdot \hat{\tau}_g + \rho_g \mathbf{g} + \bar{Q}_{mom}^p \quad (5)$$

where

$$\tau_{g\alpha\beta} = -\frac{2}{3} \rho_g k_g \mu_{\alpha\beta} + \mu_{g,eff} \left(\frac{\partial V_{g\beta}}{\partial x_\alpha} - \frac{\partial V_{g\alpha}}{\partial x_\beta} \right) - \frac{2}{3} \mu_{g,eff} \frac{\partial V_{g,r}}{\partial x_r} \delta_{\alpha\beta} \quad (6)$$

The effective viscosity is defined as follows:

$$\mu_{g,eff} = \mu_g + \mu_t \quad (7)$$

The energy conservation equation (for the Weakly compressible fluid model) is as follows:

$$\frac{\partial(\rho_g h_g(T_g))}{\partial t} + \vec{\nabla} \cdot (\rho_g V_g h_g(T_g)) \left\{ - \left(- \left(\frac{\lambda_g}{Cp_g} + \frac{\mu_t}{Pr_t} \right) \vec{\nabla} h_g(T_g) \right) \right\} + Q_{enth}^p \quad (8)$$

The turbulent Prandtl number is equal to one.

Non-evaporating particles can be calculated in laminar fluid and incompressible fluid models (Gunko et al. 2021). Those that evaporate must be calculated using models of a weakly compressible fluid or a fully compressible fluid.

The dynamics of the share is as follows (Yaropud 2021):

$$\frac{dX_p}{dt} = V_p \quad (9)$$

$$\frac{dV_p}{dt} = V_p \quad \frac{dV_p}{dt} = \frac{\pi d^2}{8m} C_{D\rho_g} |V_r| V_r + g \left(1 - \frac{\rho_g}{\rho_p} \right) \quad (10)$$

where

$$V_r = V_g - V_p \quad (11)$$

◆ the velocity of the relative bearing phase particle. The effect of the attached mass and the forces of Basset, Safman, and Magnus are not taken into account.

The speed of the carrier phase is represented as the sum of the average $\langle V_g \rangle$ and pulsating (V'_g) components (Yaropud et al. 2023):

$$V_g = \langle V_g \rangle + V'_g \quad (12)$$

At the same time, the i -th component of the pulsating component is modeled as follows:

$$V'_{gi} = \sqrt{\frac{2}{3}}k \cdot \varphi_i + V'_{dri} \quad (13)$$

The drift speed V'_{dri} is calculated as follows:

$$V'_{dri}(t + \Delta t) = V'_{dri}(t) + \Delta t \frac{1}{3} \frac{\partial k}{\partial x_i} \quad (14)$$

Integration over time is carried out from the beginning of the particle interaction with the local turbulent vortex (Horbay et al. 2018).

The process of mixing two fluids in a turbulent flow is characterized by the complex interaction between the fluid particles and turbulent eddies. Turbulent eddies create local zones of intense mixing, where mass, momentum, and energy are exchanged between particles. This means that the actual time a particle is subjected to the influence of an eddy is limited either by the eddy's lifetime or the time it takes for the particle to pass through the eddy. Both of these parameters determine how effective the mixing will be.

The interaction time of a particle with an eddy (τ_i) is the minimum of the eddy's lifetime (τ_e) and the particle's transit time through the eddy (τ_l). This approach makes sense because a particle can only interact with an eddy for as long as the eddy exists and the particle remains within the eddy.

For accurate modeling of the mixing process of two fluids, it is necessary to consider the interaction time of the particle with the eddy, defined as the minimum of the eddy's lifetime and the particle's transit time. These parameters provide a realistic description of the intensity and duration of turbulent mixing. Thermodynamic parameters, although not explicitly present in the formula, do not significantly affect the turbulent characteristics since inertial forces greatly outweigh viscous forces, especially at high Reynolds numbers, which are often characteristic of turbulent mixing. In such cases, the influence of viscosity on turbulent structures is minimal compared to inertial forces. Therefore, changes in viscosity due to changes in thermodynamic parameters will not significantly impact the turbulent process.

The time of interaction of the particle with the vortex τ_l is the minimum of two values: the life time of the vortex τ_e and the time the particle flies through the vortex τ_l :

$$\tau_l = \min(\tau_e, \tau_l) \quad (15)$$

$$\tau_e = \frac{l_e}{\sqrt{\frac{2}{3}}k} \quad (16)$$

$$\tau_l = \frac{l_e}{|V_p - \langle V_g \rangle|} \quad (17)$$

where

l_e – specific size of the vortex:

$$l_e = C_x^{3/4} \frac{k^{3/2}}{\varepsilon} \quad C_\mu = 0.09 \quad (18)$$

After the expiration of the interaction time, $\varphi_x, \varphi_y, \varphi_z$ are recalculated, V'_{dr} becomes zero. The described model of turbulent particle dispersion is a simplified version of the model proposed in research (Hrushetskyi et al. 2021; Gunko et al. 2021).

Model particles representing real particles of this size are distributed uniformly across the inlet cross-section. The user must specify the mass distribution of real particles in four size groups.

In the current version, five models for calculating C_D are implemented.

Model 1 (“Standard”):

$$C_D = \frac{21.12}{Re} + 6.3Re^{-0.5} + 0.25 \quad (19)$$

Model 2 (Kaletnik et al. 2017):

$$C_D = \frac{24}{Re} + 0.44 \quad (20)$$

Model 3 (Kaletnik et al. 2017):

$$\begin{aligned} C_D &= \frac{24}{Re} + 4Re^{-13} & Re < 1000 \\ C_D &= 0.44 & Re \geq 1000 \end{aligned} \quad (21)$$

Model 4 Stein (Kaletnik et al. 2017):

$$C_D = \frac{24}{Re} + 5.48Re^{-0.573} + 0.36 \quad (22)$$

Model 5:

$$\begin{aligned} C_D &= \frac{24}{Re} + 4.5 & Re < 1 \\ C_D &= 25 - 24lgRe + 9.06821lg^2 Re - 1.7713lg^3 Re + 0.1718lg^4 Re - 0.0065lg^5 Re & 1 \leq Re \leq 3000 \\ C_D &= 0.4 & Re > 3000 \end{aligned} \quad (23)$$

When $Re < 0.1$, the drag coefficient is always calculated according to Stokes:

$$C_D = \frac{24}{Re} \quad (24)$$

It is assumed that the heat transfer inside the particle is infinitely fast. Conservation of mass is as follows:

$$\frac{dm}{dt} = -\dot{m}\pi d^2 \quad (25)$$

$$\dot{m} = \frac{Sh \mu_g}{Sc d} \quad (26)$$

In the current version, five models for calculating value F are implemented (Paliy et al. 2021; Shevchenko et al. 2021; Shevchenko and Aliiev 2020).

Model 1:

$$F = In \left[+ \frac{Y_{1sat}(T_p) - Y_1}{Y_{sat}(T_p)} \right] \quad (27)$$

Model 2:

$$F = \frac{Y_{1sat}(T_p) - Y_1}{1 - Y_{1sat}(T_p)} \quad (28)$$

Model 3:

$$F = \frac{Y_{1sat}(T_p) - Y_1}{1 - Y_{1sat}(T_p)} \cdot \frac{1}{1 + C_{Pvol} \frac{T_g - T_p}{h_{lat}(T_p)}} \quad (29)$$

Model 4:

$$F = Y_{1sat}(T_p) - Y_1 \quad (30)$$

Model 5:

$$F = (Y_{1sat}(T_p) - Y_1) \cdot \frac{1}{1 + C_{Pvol} \frac{T_g - T_p}{h_{lat}(T_p)}} \quad (31)$$

At $Y_{1sat}(T_p) > 0.99$ and $T_g > T_{p,boil}$ drops evaporate in boiling mode:

$$\dot{m} = Nu \frac{\lambda_g}{d} \frac{T_g - T_{p,boil}}{h_{lat}(T_{p,boil})} \quad (32)$$

Substance 1 can condense on the surface of the droplets. Conservation of energy (equation for particle temperature) is as follows (Hraniak et al. 2022):

$$\frac{dT_p}{dt} = (\dot{q} - \dot{m}h_{lat}(T_p)) \frac{6}{d\rho_p C_p} \quad (33)$$

$$\dot{q} = Nu \frac{\lambda_g}{d} (T_g - T_p) + \sigma_{rad} \varepsilon_{rad} (T_g^4 - T_p^4) \quad (34)$$

The current version implements two models for calculating Sherwood and Nusselt numbers. Klift model:

$$\begin{aligned} Sh &= 1 + (1 + ReSc)^{1/3}, & Re \leq 1 \\ Sh &= 1 + (1 + ReSc)^{1/3} Re^{0.077}, & Re > 1 \\ Nu &= 1 + (1 + RePr)^{1/3}, & Re \leq 1 \\ Nu &= 1 + (1 + RePr)^{1/3} Re^{0.077}, & Re > 1 \end{aligned} \quad (35)$$

Frossling model:

$$\begin{aligned} Sh &= 2 + 0.552 Re^{1/2} Sc^{1/3} \\ Nu &= 2 + 0.552 Re^{1/2} Pr^{1/3} \end{aligned} \quad (36)$$

Interaction of the drop with the wall

For the drops near the wall, the Weber number is determined:

$$We = \frac{\rho_d d V_{dh}^2}{\sigma(T_d)} \quad (37)$$

- ◆ In the sticking mode, the particle slowly approaches the wall, sticks, and flows into the film
Sticking mode: $We < 5$
- ◆ At higher normal velocities, the drop bounces off the wall.
Bounce mode: $5 < We < 10$
- ◆ This is followed by an infusion mode that is similar to the sticking mode
Infusion mode: $10 < We, S < 1$

$$S = \frac{Re}{24 \cdot La^{0.419}}, \quad Re = \frac{\rho_d d V_{dn}}{\mu_d(T_d)}, \quad La = \frac{\rho_d d \sigma(T_d)}{\mu_d(T_d)} \quad (38)$$

Finally, the most intense interaction takes place in the sprinkling mode, which is characterized by the injection of a part of the liquid into the film and the return of secondary (significantly smaller) droplets to the carrier phase (Fig. 1).

The empirical ratio for the mass fraction of the liquid poured into the film is as follows:

$$\eta = S^{-0.6} \quad (39)$$

The empirical ratio for the average diameter of secondary drops is as follows:

$$\ln \frac{d_{splash}}{d_0} = -2 \frac{d_0}{d_{ref}} - 0.05S, \quad d_{ref} = 4066 \mu m \quad (40)$$

where:

- d_0 – the diameter of the drop before it collides with the wall,
- d_{splash} – the diameter of the droplets formed during the collision.

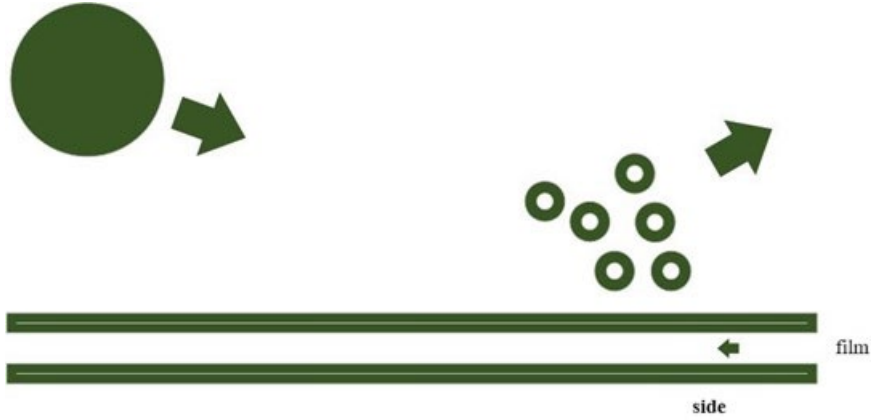


Fig. 1. Sprinkling mode: $S > 1$

Rys. 1. Tryb zraszania: $S > 1$

2. Results and discussion

Before considering the solution of convective transfer equations in the multidimensional case, a numerical scheme for calculating a one-dimensional equation of the convective transfer of the scalar quantity f with the speed $u(x)$ will be developed (Fig. 2) (Horbay et al. 2018; Galushchak et al. 2023).

Let's introduce a grid with a constant step in space

$$x_{i+1/2} \quad i = 0, 1, \dots, N$$

where i -th finite volume is bounded by the sides with coordinates $x_{i-1/2}$, $x_{i+1/2}$. Volume V_i that corresponds volume V_i is bounded by the sides with $x_{i-1/2}x_{i+1/2}\delta_{1+1/2}$. Here $\delta_{1+1/2}$ is the length of the inverse characteristic that leaves the point $x_{i+1/2}$ at the moment of time t_{n+1} and is directed to the moment of time t_n . The value $\delta_{1+1/2}$ is determined by the equation

$$T = \int_{x_{i+1/2}-\delta_{1+1/2}}^{x_{i+1/2}} \frac{dx}{u(x)} \quad (41)$$

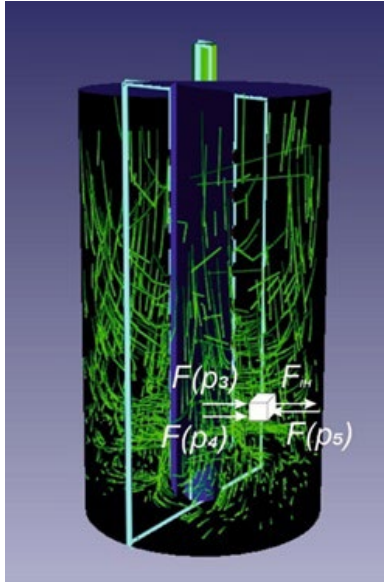


Fig. 2. Simulation of the movement of liquid flows in the mixer by the FlowVision program

Rys. 2. Symulacja ruchu przepływów cieczy w mieszalniku za pomocą programu FlowVision

To the first approximation, a slowly changing velocity along the x-axis can be assumed, which is $\delta_{1+1/2} = \tau u_{i+1/2}$; the length of the characteristic can be specified using the predictor-corrector method.

The one-dimensional equation of purely convective transport in Lagrangian form is as follows:

$$f_i^{n+1} = \int_{x_{i-1/2} - \delta_{i-1/2}}^{x_{i+1/2} - \delta_{i+1/2}} f(x, t^n) dx \quad (42)$$

According to the equation, the problem of solving the convective transmission equation turns into the problem of reconstructing the function $f(x, t)$ within the finite volume according to its average values. The quality of reconstruction determines the circuit behavior: a monotonous reconstruction will give a monotonous circuit, and a high accuracy of the reconstruction will give a low level of chain diffusion.

Diagrams generated using the Lagrange representation are stable for any integration steps τ (any Courant numbers $CFL = \delta_{i-1/2}/h$). Time integration accuracy is determined by calculating the length of the inverse characteristic (Kaletnik et al. 2020a, 2020b).

Different reconstructions $f(x, t)$ within a finite volume from the linear continuous class are shown in the figure. Reconstruction I by the parts of the constant function leads to the well-known counter flow scheme of the first-order approximation. Reconstruction II introduces the slope of the function $f(x)$ inside V_i , which is calculated using a symmetric finite difference. This reconstruction has the second order of approximation but is not uniform.

Monotonic reconstruction III is obtained by calculating the slope of $f(x)$ within V_i as a minimum of slopes calculated from the finite differences on both sides of the finite volume (Fig. 3).

$$f(x) = +0.5(f_{i+1} - f_{i-1}) \frac{(x_i - x)}{h} \quad (43)$$

$$f(x) = f_i \quad (44)$$

$$f(x) = f_i + f_{xi} \frac{(x_i - x)}{h} \quad (45)$$

where $f_{xi} = \min(f_{i+1} - f_i, f_i - f_{i-1})$ at $(f_{i+1} - f_{i-1}) > 0$ (46)

where $f_{xi} = \max(f_{i+1} - f_i, f_i - f_{i-1})$ at $(f_{i+1} - f_{i-1}) < 0$ (47)

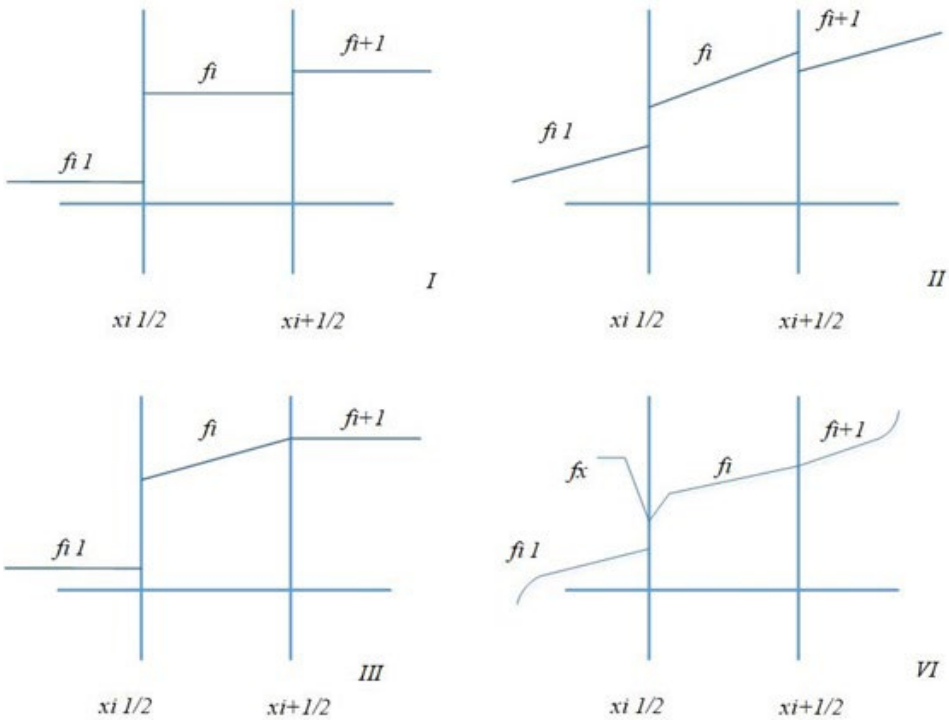


Fig. 3. Types of linear reconstruction $f(x)$

Rys. 3. Rodzaje rekonstrukcji liniowej $f(x)$

Flow Vision uses a more complex linear reconstruction with an additional point (reconstruction IV). It has the following form:

$$f(x) = \begin{cases} f_{ri} + f_{xn}(x_{i+1/2} - x), & x \geq x_{i+1/2} - l \\ f_{li} + f_{xli}(x - x_{i-1/2}), & x \leq x_{i+1/2} - l \end{cases} \quad (48)$$

where l is the distance from the side $x_{i+1/2}$ to the additional point f_{ri}, f_{li} , i.e., the values of the reconstruction function on the left and right borders of the finite volume. The values of f_{ri}, f_{li} are determined from the position of function f in the Taylor series:

$$f(x) = (x_{i+1/2})f'_x \Delta x + \frac{1}{2} f''_{xx} \Delta x^2 + \frac{1}{3!} f'''_{xxx} \Delta x^3 \theta(\Delta x^4) \quad (49)$$

$$\Delta x = x - x_{i+1/2} \quad (50)$$

Its coefficients can be found using definitions of the average value of the function of the i -th finite volume and its nearest neighbors $i-1$ and $i+1$. Thus, we have:

$$f_{ri} = \frac{1}{2}(f_{i+1} + f_i) - \frac{1}{6}(f_{i+1} - 2f_i + 2f_{i-1}) \quad (51)$$

$$f_{li} = \frac{1}{2}(f_i + f_{i-1}) - \frac{1}{6}(f_{i+1} - 2f_i + 2f_{i-1}) \quad (52)$$

To achieve uniformity of the reconstruction, the values of f_{ri}, f_{li} are limited to the average values of neighboring finite volumes:

$$\begin{cases} f_i \leq f_{ri} \leq f_{i+1}, & \text{when } f_{i+1} - f_i \geq 0 \\ f_i > f_{ri} > f_{i+1}, & \text{when } f_{i+1} - f_i < 0 \end{cases} \begin{cases} f_{i-1} \leq f_{li} \leq f_i, & \text{when } f_i - f_{i-1} \geq 0 \\ f_{i-1} > f_{li} > f_i, & \text{when } f_i - f_{i-1} < 0 \end{cases} \quad (53)$$

Distance l and the derivatives f_{xri}, f_{xli} on the left and right sides of V_i are as follows

$$l = \frac{f_i - f_{li}}{f_{ri} - f_{li}}, \quad f_{xri} = \frac{f_{ri} - f_i}{l}, \quad f_{xli} = \frac{f_i - f_{li}}{1-l} \quad (54)$$

To check the true accuracy, the solution to Leonard's test problem is to be considered. This test consists of the calculation of one-dimensional motion with a constant speed of three profiles, namely, a step, a half period of a sine square, and a half ellipse. The figure shows a comparison of numerical solutions based on reconstructions I-IV with the exact solution (Kaletnik et al. 2020b). The results are displayed at time step 120 when calculated using CFL = 0.5.

Schemes I and III are uniform but have an unacceptably large diffusion scheme. Scheme II, created due to non-monotonic reconstruction, has an oscillating solution. The scheme with re-

construction IV is the most accurate one. It has the property of uniformity, along with the fine diffusion scheme.

Modeling of three-dimensional transfer

As for equation (54) of the section, the subgrid method of the separating power of geometry of three-dimensional convective-diffusion transfer of scalar quantity is to be considered. The equation can be divided into two parts as follows:

$$(1) f_i^n = \frac{1}{V_i} \int_{V_i \cap \Omega_i} f^n dV \quad (55)$$

$$f_i^{n+1} = f_i^n - \frac{1}{V_i} \left(\sum_g G_g (f_i^{n+1}) + D(f_i^{n+1}) \right) \quad (56)$$

Equation (55) describes the convective transfer of the quantity f . It is stable for any time step. Equation (56) describes diffusion processes (term with D) and boundary conditions (term with Gg). To get rid of the dependence on τ in (55), the equation is written in an implicit form.

A three-dimensional function $f(x)$ in (57) is reconstructed using the superposition of three functions $f^{n,k}(x_k)$, and each of them is a one-dimensional reconstruction along the x_k axis of the Cartesian coordinate system:

$$(3) f_i(x) = \sum_{k=1}^3 f^k(x_k) - 2f_i^n \quad (57)$$

Firstly, the explicit equation (1) is solved for the intermediate variable f^n . Then, one of the standard methods, e.g., the upper relaxation method, solves the implicit equation (52) for f^{n+1} .

Let's consider the numerical integration of the Navier-Stokes equations. The equation for the moving volume is as follows

$$\int_{V_i} \rho V dV = \int_{\Omega_i} \rho dV \quad (58)$$

$$\int_{V_i} \rho V dV - \int_{\Omega_i} \rho dV = - \int_{\tau} \int_S P dS dt + D \quad (59)$$

where:

- S – the surface of the volume Ω ,
- V – the fluid velocity field,
- P – pressure,
- ρ – density,
- D – denotes the terms in the Navier-Stokes equation that describe viscous stresses, gravity, etc.

Additional equations describing the change in density and turbulent transport are needed to close the system of equations. The type of these equations depends on the physical formulation of the problem and is not considered here.

The difference analog of the Navier-Stokes equations can be expressed as it is given below.

The unknowns in this equation are V^{n+1} and P^{n+1} . Then, additional terms in (61) are added and subtracted as follows

$$\begin{aligned} & (V_i^{n+1} + \bar{V} - \bar{V})V_i\rho^{n+1} - \int_{\Omega_1} \rho^n V^n dV = \\ & = -T \left(\sum_s P_s^{n+1} s - \sum_b P_b^n b + \sum_b P_b^n b \right) D_i(V) \end{aligned} \quad (60)$$

$$V_i\rho^{n+1} - \int_{\Omega_1} \rho^n V^n dV = -\sum_b P_b^n b + D_i(\bar{V}) \quad (61)$$

This equation is divided into two parts

$$(2) V_i^{n+1} V_i \rho^{n+1} - \int_{\Omega_1} \rho^n V^n dV = -T \left(\sum_b P_b^{n+1} s + D_i(V) \right) \quad (62)$$

$$(3) (V_i^{n+1} - \bar{v}) V_i \rho^{n+1} = \sum_s P_s^{n+1} + \sum_b P_b^n b \quad (63)$$

It can be seen that equation (62) is again a discrete analog of the Navier-Stokes equations. However, unlike the original analog of (61), (62) uses the pressure field made at the previous time step.

Vector equation (62) is three convective diffusion transfer equations for three fluid velocity components. These equations are solved using the method outlined in the previous section. For this, (63) is divided as follows

$$V_i = \frac{1}{V_i \rho^{n+1}} \left(V^n dV - T \sum_b P_b^n b \right) \quad (64)$$

To determine the pressure field, the state of incompatibility of the fluid, which it flows from is to be considered

$$\sum_s V_s^{n+1} s = 0 \quad (65)$$

where V^{n+1} – the velocity value at the boundary of the final volume V . To obtain the expression for V^{n+1} , let's write the analog of equation (65), obtained by integrating the Navier-Stokes equations on the moving face of the volume Ω . For a face of this volume that coincides with the faces b at $t = t_n$ and with s at $t = t_{n+1}$ the expression for V^{n+1} has the form

$$V_s^{n+1} = \bar{V}_s + \frac{T}{P_b^{n+1}} (\nabla P^{n+1}) \Big| - \frac{T}{P_s^{n+1}} (\nabla P^{n+1}) \Big| \quad (66)$$

Having substituted V^{n+1} in (6), we get the equation for determining the pressure

$$\sum_s \frac{T}{P_s^{n+1}} (\nabla P^{n+1}) \Big|_s = \sum_s \bar{V}_s s + \sum_b \frac{T}{P_s^{n+1}} (\nabla P^n) \Big|_b \quad (67)$$

In the second term on the right side of equation (68), the summation is done on the faces b of the volume Ω_i , and not on $P_b^{n+1} = P_s^{n+1}$ faces s of the volume V_i , since ∇P^n is defined for the volume Ω_i . Values for the corresponding faces b and s .

After finding the pressure field P^{n+1} from (68), the velocity field V^{n+1} is calculated.

It is well known that the pressure field fluctuates when solving the equations of motion of an incompressible fluid on undistorted grids. In FlowVision, this difficulty is overcome by introducing into the pressure equation (67) the difference between the representation of the pressure gradient of the second and fourth order of accuracy according to the work.

Let's consider the general form of diffusion-type equations:

$$\frac{\partial}{\partial t} (TC \cdot f) = \frac{1}{PC} \nabla (DC \cdot \nabla f) + SST \quad (68)$$

and convective-diffusion type

$$\frac{\partial}{\partial t} (TC \cdot f) + \nabla (CC \cdot f) = \frac{1}{PC} \nabla (DC \cdot \nabla f) + SST \quad (69)$$

where:

- t – time,
- ∇ – gradient operator,
- V – velocity vector.

The values of TC (Time Coefficient), CC (Convective Coefficient), PC (Prediffusion Coefficient), and DC (Diffusion Coefficient) coefficients of the equation at the corresponding ones determine the derivatives, SST (Scalar Source Term) determine the output term.

The proposed mixer model was used to simulate the working cavity of the device, which was filled with a liquid, indicating all the outlet, inlet, and physicochemical characteristics of the fuel (Fig. 4–5).

Before starting the simulation, the initial position of the particle in the coordinate system is determined, e.g., the part of the mixer in which it is located. FlowVision CFD uses Navier-Stokes equations to model fluid motion. These equations describe the change in fluid velocity from time to time and determine how the flow affects particle motion. The particle interacts with the liquid phase through the exchange of mass, momentum, and energy. As a result of this interaction, the particle can change its speed and direction of movement depending on the characteristics of the liquid. Particle parameters such as mass, size, and shape also affect its motion. These parameters are considered in the calculations to determine the particle's trajectory. In some cases, a particle

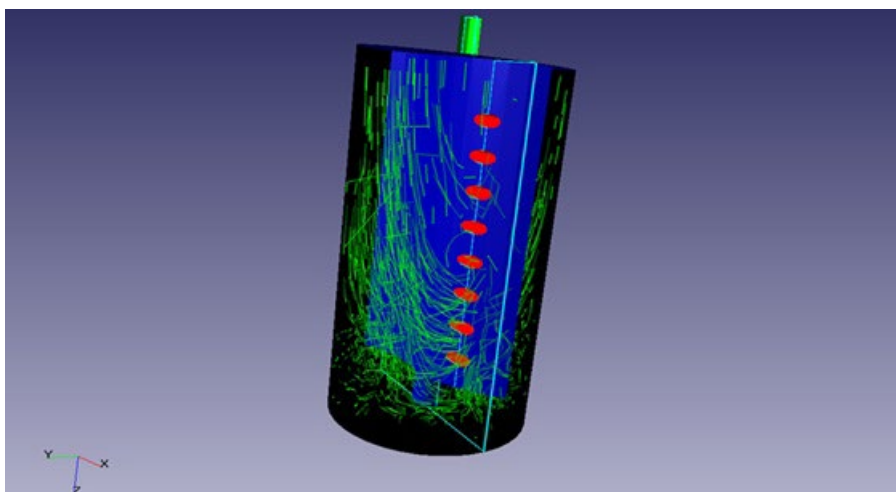


Fig. 4. Modeling of the working cavity of the mixer filled with diesel and biofuel

Rys. 4. Modelowanie komory roboczej mieszalnika wypełnionego olejem napędowym i biopaliwem

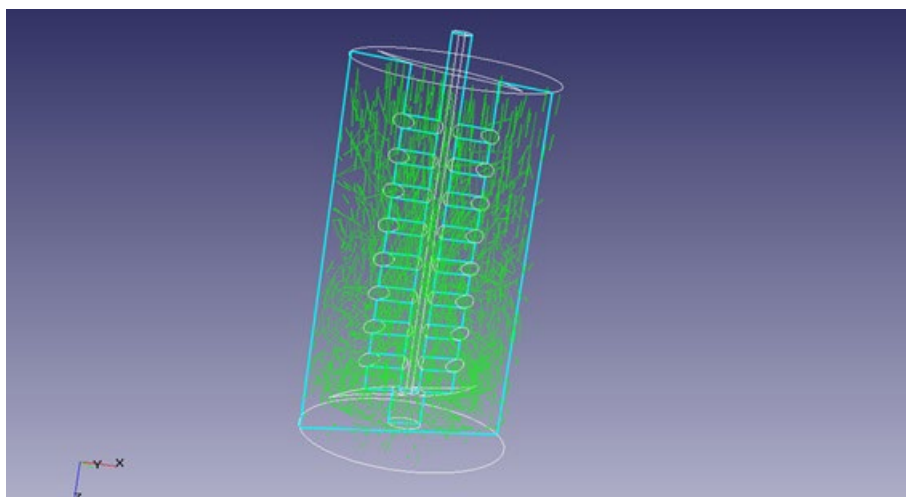


Fig. 5. Simulation of the fuel particle motion in the volume of the mixer

Rys. 5. Symulacja ruchu cząstek paliwa w objętości mieszalnika

may stop, or its status may change due to interaction with the liquid phase, e.g., during adhesion to a surface or a change in the aggregate state. The simulation of the particle motion continues until the end time is reached or until certain criteria for stopping the particle are reached, which can be specified in the model.

The particle motion is calculated in FlowVision CFD based on the equations of fluid motion, the physical properties of the particle, and the interaction with the fluid phase. This information

allows us to study the trajectory of particle motion during the mixing of diesel and biofuel in a defined volume or mixer.

The interaction of the speed and pressure of particles when mixing diesel and biofuel is determined by the laws of liquid flow and calculations of the Navier-Stokes equations. The relationship between these two parameters plays a key role in determining the motion and distribution of particles in the system (Fig. 6).

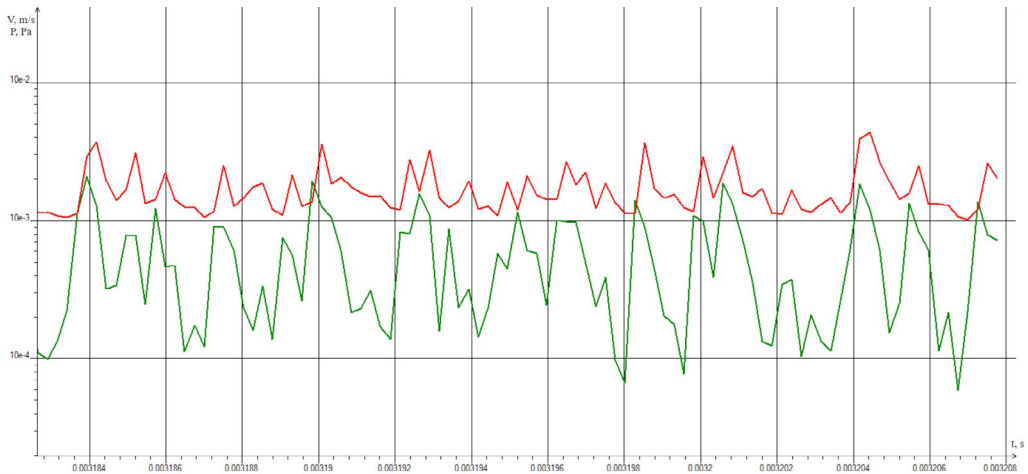


Fig. 6. Dependence of pressure and velocity of particles in time when mixing diesel fuel and biofuel

Rys. 6. Zależność ciśnienia i prędkości cząstek w czasie podczas mieszania oleju napędowego i biopaliwa

Particles that move with the fluid are carried with the corresponding velocity of the fluid. If there is a change in the velocity of the fluid in the system, this will also affect the velocity and distribution of the particles.

Turbulence in the fluid flow can lead to changes in pressure and velocity at various points in the system. This can cause particles to move from a high-pressure area to a low-pressure area or vice versa.

The particle motion potential is determined by the physical properties of the fluid, the properties of the particles, the boundary conditions, and the parameters of the model in which they are analyzed. Modeling this movement allows us to study the influence of various factors on the distribution of particles in the system during their mixing of diesel and biofuel (Fig. 7).

The physical properties of the fluid, such as density, viscosity, temperature, and pressure, determine the environment in which the particles move. Particles will move in the direction of decreasing potential energy, which can be caused by a pressure gradient or fluid density.

This interaction can change the speed and direction of the particle motion.

Gravitational forces can also affect the motion of particles, especially in cases where the liquid phase is under the influence of gravity.

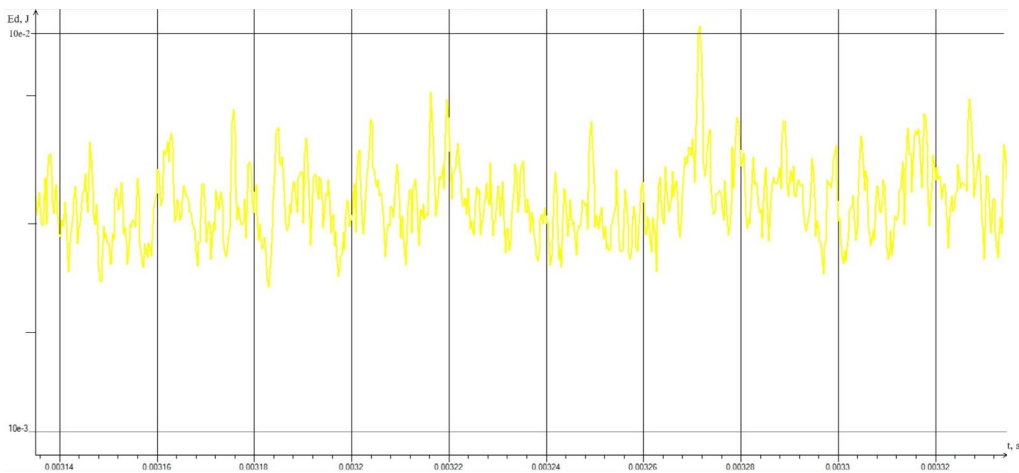


Fig. 7. The potential of particle motion when mixing diesel and biofuel

Rys. 7. Potencjał ruchu cząstek podczas mieszania oleju napędowego i biopaliwa

In turbulent modes of fluid movement, particles can be in complex jet flows, which can lead to their movement and change in speed.

Depending on the properties of particles and liquid, adhesion (binding) of particles to other surfaces or aggregation (uniting) of particles together may occur.

The movement of particles can be limited by the geometry of the mixer or the volume in which they are considered. These boundary conditions can affect the motion of particles and their potential energy.

To obtain accurate data on pressure changes when mixing diesel and biofuel in FlowVision CFD, it is necessary to perform calculations using appropriate flow models and set initial conditions and parameters corresponding to your specific task (Fig. 8).

In principle, when diesel and biofuel are mixed in the mixer, the pressure can change in the following ways. If the biofuel volume is greater than the volume of diesel fuel, and they are mixed in a narrow channel or constricted product, then an increase in pressure may occur in this area. If biofuel has a lower density or viscosity than diesel and they are mixed in a narrow channel, a pressure drop may occur due to a reduction in flow resistance. In many cases, the pressure can remain constant if the amount of diesel and biofuel, as well as the mixing conditions, are balanced in such a way that no significant pressure changes occur. Turbulence can be observed in the mixing zone, which can lead to local changes in pressure and the creation of pressure gradients depending on the speed and direction of the flow.

To obtain data on the change in the speed of the particle motion when mixing diesel and biofuel in FlowVision CFD, we perform calculations using appropriate flow models, set initial conditions, and take into account the physical properties of both components. The simulation results will allow us to understand how the speed of particles changes and how it affects the process of mixing diesel and biofuel (Fig. 9).

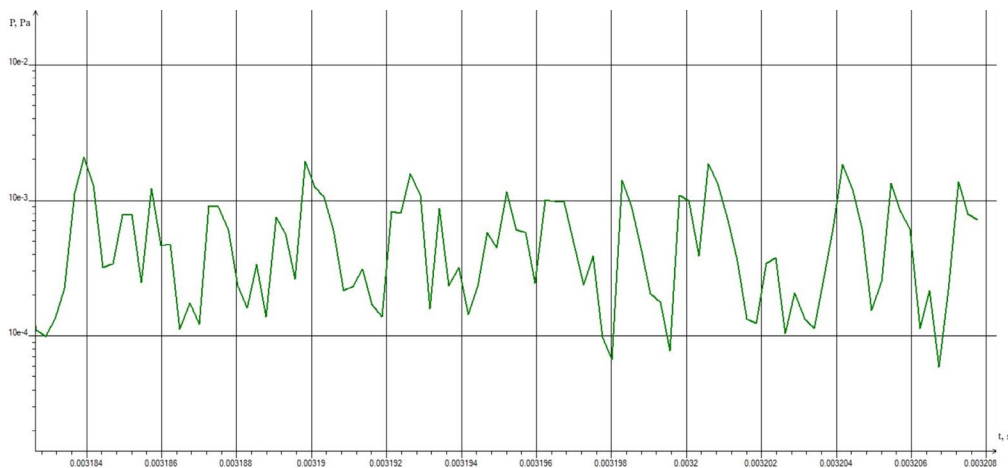


Fig. 8. Pressure change in the volume of the mixer when mixing diesel fuel and biofuel

Rys. 8. Zmiana ciśnienia w objętości mieszalnika podczas mieszania oleju napędowego i biopaliwa

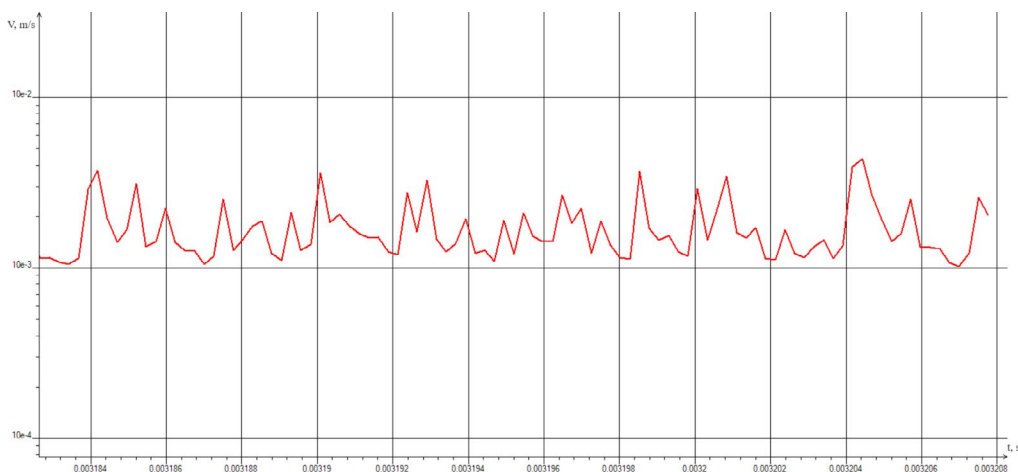


Fig. 9. Change in particle velocity in the volume of the mixer when mixing diesel and biofuel

Rys. 9. Zmiana prędkości cząstek w objętości mieszalnika podczas mieszania oleju napędowego i biopaliwa

In principle, since the fuels have different viscosity or density, the changes in the speed of the particle motion can be observed when mixing diesel and biofuel. Hence, the turbulent flow in the mixer may increase the speed of particles to achieve a uniform distribution of components. In some cases, when biofuel has a higher viscosity than diesel, a reduction in particle velocity may occur due to flow resistance. Under more uniform conditions, particle motion can remain constant even if the properties and parameters of the fuels are adjusted to compensate for the change in velocity. The speed of particles can vary locally due to turbulence and mixing in different areas of the mixer.

Conclusion

Using experimental, theoretical, and numerical approaches, scientists have found out that various parameters of the blade mixer geometry, such as the shape of the blades, the angle of inclination, their size, and location, can change the distribution of turbulence in the fluid flow and the intensity of mixing. Optimization of the mixer geometry can improve the quality and efficiency of mixing processes, as well as reduce energy and resource costs. Studies confirm that developed turbulence is achieved when a blade diameter is 0.015 m, which can be useful for certain applications where a high level of turbulence is required. However, to ensure optimum efficiency, smooth operation, and intensive mixing, a blade diameter of 0.055 m has been found to be the most structurally advantageous. This can be a compromise between achieving efficient mixing and maintaining stability and economy.

The choice of geometric dimensions of the mixer is made taking into account the type of fuel, design features, and calculation data. This highlights the importance of a balanced approach when designing mixers for specific applications. Increasing the size of the blades by more than 0.075 m can lead to a decrease in strength, difficulty in manufacturing, and a decrease in rotation speed, which will negatively affect the performance of the mixer as a whole.

This research was supported and funded by the Ministry of Education and Science of Ukraine under grant No. 0122U000844.

The Authors have no conflicts of interest to declare.

References

- ALIEV et al. 2021 – ALIEV, E., PAVLENKO, S., GOLUB, G. and BIELKA, O. 2021. Research of mechanized process of organic waste composting. *Agraarteadus, Journal of Agricultural Science* 2022, XXXIII (1), pp. 21–32, DOI: 10.15159/jas.22.04.
- BANDURA et al. 2023 – BANDURA, V., BEZBAH, I., KUPCHUK, I. and FIALKOVSKA, L. 2023. Innovative methods of drying rapeseeds using microwave energy. *Polityka Energetyczna – Energy Policy Journal* 26(2), pp. 217–230, DOI: 10.33223/epj/163328.
- BURLAKA et al. 2021 – BURLAKA, S., YAROPUD, V. and ZDYRKO, N. 2021. Recommendations for evaluation and diagnosis of diesel engine when using biofuels. *Bulletin of Khmelnytsky National University* 4 (299), pp. 169–173 (in Ukrainian).
- COSTA, M. and PIAZZULLO, D. 2018. Biofuel Powering of Internal Combustion Engines: Production Routes, Effect on Performance and CFD Modeling of Combustion. *Frontiers in Mechanical Engineering* 4(9), pp. 1–14, DOI: 10.3389/fmech.2018.00009.
- GALUSHCHAK et al. 2023 – GALUSHCHAK, O., BURLAKA, S., KUPCHUK, I., BONDARENKO, V. and GONTARUK, Y. 2023. Environmental indicators of the operation of a diesel generator running on a mixture of bio-fuels. *Polityka Energetyczna – Energy Policy Journal* 26(4), pp. 195–208, DOI: 10.33223/epj/170759.
- GALUSHCHAK, O. 2015. The method of control of the diesel power supply system when using the dynamic regulation of the percentage composition of the mixture of fuels. *Scientific works of Vinnytsia National Technical University. Mechanical engineering and transport* 3, pp. 1–8.

- GALUSHCHAK, O.O. and GALUSHCHAK, D.O. 2014. Algorithm of operation of electronic engine control unit in determining the percentage of biodiesel and diesel fuels. Collection of abstracts of the International scientific-practical conference “*The latest technologies for the development of construction, production, operation, repair and examination of the car*”, October 15–16, Kharkiv, pp. 215–216.
- GUNKO et al. 2021 – GUNKO, I., HRANIAK, V., YAROPUD, V., KUPCHUK, I. and RUTKEYVCH, V. 2021. Optical sensor of harmful air impurity concentration. *Przegląd Elektrotechniczny* 97(7), pp. 76–79, DOI: 10.15199/48.2021.07.15.
- GUNKO I. et al. 2021 – GUNKO, I., BABYN, I., ALIEV, E., YAROPUD, V. and HRYTSUN, A. Research into operating modes of the air injector of the milking parlor flushing system. *U.P.B. Sci. Bull., Series D* 83(2), pp. 297–310. [Online] https://www.scientificbulletin.upb.ro/rev_docs_arhiva/rez4fb_469127.pdf [Accessed: 2024-05-03].
- HORBAY et al. 2018 – HORBAY, O., POLIAKOV, A., HRECHANIUK, M. and VISHTAK, I. 2018. Dynamic regulation of the percentage composition of the mix diesel and biodiesel fuel. *Transport Problems* 13(2), pp. 59–67, DOI: 10.20858/tp.2018.13.2.6.
- HRANIAK et al. 2022 – HRANIAK, V.F., MATVIYCHUK, V.A. and KUPCHUK, I.M. 2022. Mathematical model and practical implementation of transformer oil humidity sensor. *Electronics* 26(1), pp. 3–8, DOI: 10.53314/ELS2226003H.
- HRUSHETSKYI et al. 2021 – HRUSHETSKYI, S., YAROPUD, V., KUPCHUK, I. and SEMENYSHENA, R. 2021. The heap parts movement on the shareboard surface of the potato harvesting machine. *Bulletin of the Transilvania University of Braşov. Series II: Forestry, Wood Industry, Agricultural Food Engineering* 14(1), pp. 127–140, DOI: 10.31926/but.fwiafe.2021.14.63.1.12.
- KALETNIK et al. 2017 – KALETNIK, H., PILVERE, I., NIKOLAENKO, S. and BULGAKOV, V. 2017. Investigation of biofuel production possibilities for stabilisation of agro-industrial complex of Ukraine. *Engineering For Rural Development*, Jelgava, 24–26.05.2017, pp. 1250–1256, DOI: 10.22616/ERDev2017.16.N273.
- KALETNIK et al. 2020a – KALETNIK, G., HONCHARUK, I. and OKHOTA, Y. 2020a. The Waste-free production development for the energy autonomy formation of Ukrainian agricultural enterprises. *Journal of Environmental Management and Tourism* 11(3), pp. 513–522, DOI: 10.14505//jemt.v11.3(43).02.
- KALETNIK et al. 2020b – KALETNIK, H., MAZUR, V., GUNKO, I., RYABOSHAPKA, V., BULGAKOV, OLT, J., RAIDE, V. and LIVES, R. 2020b. Study on performance of compression engine operated by biodiesel fuel. *Agronomy Research* 5, pp. 862–887, DOI: 10.15159/AR.20.027.
- KALETNIK, G. and YAROPUD, V. 2021. Theoretical studies of air losses of air heat exchanger of indirect-evaporative type of livestock rooms. *Machinery and Energetics* 12(4), pp. 35–41, DOI: 10.31548/machenergy2021.04.035.
- KALETNIK, H. and YAROPUD, V. 2023. Research of pressure losses and justification of forms of side-evaporative heat exchangers channels in livestock premises. *Przegląd Elektrotechniczny* 99(7), pp. 247–252, DOI: 10.15199/48.2023.07.46.
- KUPCHUK et al. 2022 – KUPCHUK, I., BURLAKA, S., GALUSHCHAK, A., YEMCHYK, T., GALUSHCHAK, D. and PRYSIAZHNIUK, Y. 2022. Research of autonomous generator indicators with the dynamically changing component of a two-fuel mixture. *Polityka Energetyczna – Energy Policy Journal* 25(2), pp. 147–162, DOI: 10.33223/epj/150746.
- PALIY et al. 2021 – PALIY, A., ALIEV, E., NANKA, A., BOGOMOLOV, O., BREDIXIN, V., PALIY, A., SHKROMADA, O., MUSIENKO, Y., STOKIY, A. and GREBENIK, N. Identifying changes in the technical parameters of milking rubber under industrial conditions to elucidate their effect on the milking process. *Eastern-European Journal of Enterprise Technologies* 3(1) (111), pp. 21–29, DOI: 10.15587/1729-4061.2021.231917.

- SHEVCHENKO et al. 2021 – SHEVCHENKO, I., ALIEV, E., VISELGA, G. and KAMINSKI, J. 2021. Modeling Separation Process for Sunflower Seed Mixture on Vibro-Pneumatic Separators. *Mechanika* 27(4), pp. 311–320, DOI: 10.5755/j02.mech.27647.
- SHEVCHENKO, I. and ALIEV, E. 2020 – Improving the efficiency of the process of continuous flow mixing of bulk components. *Eastern-European Journal of Enterprise Technologies* 6/1 (108), pp. 6–13, DOI: 10.15587/1729-4061.2020.216409.
- YAROPUD et al. 2023 – YAROPUD, V., ALIEV, E., MAZUR, I. and BURLAKA, S. 2023. Simulating the process of operation of vortex layer electromagnetic apparatus with ferromagnetic working elements. *Przegląd Elektrotechniczny* 99(9), pp. 64–71, DOI: 10.15199/48.2023.09.11.
- YAROPUD, V. 2021. Analytical study of the automatic ventilation system for the intake of polluted air from the pigsty. *Scientific Horizons* 24(3), pp. 19–27, DOI: 10.48077/scihor.24(3).2021.19-27.

Serhii BURLAKA, Ihor KUPCHUK, Tetiana BORETSKA, Yaroslav GONTARUK, Maryna MELNYK

Optymalizacja procesu mieszania oleju napędowego i biopaliwa w mieszalniku łopatkowym w celu poprawy jakości mieszanki

Streszczenie

W niniejszym artykule analizowany jest ważny aspekt procesów technologicznych – proces mieszania oleju napędowego i biopaliwa w specjalnie zaprojektowanym mieszalniku łopatkowym. Głównym celem jest optymalizacja i poprawa jakości powstałej mieszanki. Wykorzystanie w badaniu programu FlowVision CFD (Computational Fluid Dynamics) ma ogromne znaczenie i pozwala na osiągnięcie znaczących wyników w analizie i optymalizacji procesu mieszania oleju napędowego z biopaliwem. W kontekście wielu procesów przemysłowych i technologicznych, gdzie ważną rolę odgrywa sprawne mieszanie cieczy, duże znaczenie ma mieszanie turbulентne. Optymalne mieszanie nie tylko poprawia jakość produktów, ale także zapewnia jednolitość złożonych reakcji, a także pomaga skrócić czas zakończenia procesu. Należy podkreślić, że badania skupiają się nie tylko na ilościowych aspektach mieszania, ale także na analizie wpływu geometrii mieszadła na turbulენტną charakterystykę przepływu. Może to doprowadzić do opracowania nowych konstrukcji mieszadeł mających na celu maksymalizację efektywności procesu mieszania paliw, co w efekcie pozwoli zaoszczędzić zasoby i zmniejszyć emisję szkodliwych substancji do atmosfery. Badania te otwierają perspektywy dalszego rozwoju w dziedzinie technologii mieszania paliw, co może prowadzić do realnej poprawy produkcji i zrównoważonego rozwoju. Odkrycie nowych metod optymalnego mieszania cieczy w specjalnie zaprojektowanych mieszadłach może przesądzić o przyszłości efektywności energetycznej i ograniczeniu negatywnego wpływu na środowisko.

SŁOWA KLUCZOWE: geometria mieszalnika, rozwiązanie numeryczne, turbulencja, gradient ciśnienia, przepływy turbulენტne